

Investigating the Effect of Added Salt on the Chain Dimensions of Poly(ethylene oxide) through Small-Angle Neutron Scattering

Whitney S. Loo,[†] Katrina I. Mongcopa,[†] Daniel A. Gribble,^{†,‡} Antonio A. Faraone,[§] and Nitash P. Balsara^{*,†,‡,||}

[†]Department of Chemical and Biomolecular Engineering, University of California Berkeley, Berkeley, California 94720, United States

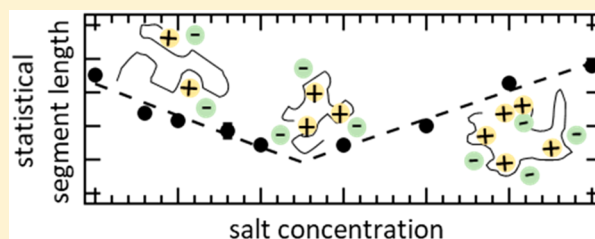
[‡]Materials Sciences Division, Lawrence Berkeley National Lab, Berkeley, California 94720, United States

[§]National Institute of Standards and Technology Center for Neutron Research, Gaithersburg, Maryland 20899, United States

^{||}Joint Center for Energy Storage Research (JCESR), Lawrence Berkeley National Lab, Berkeley, California 94720, United States

Supporting Information

ABSTRACT: We have measured the effect of added salt on the chain dimensions of mixtures of poly(ethylene oxide) (PEO) and lithium bis(trifluoromethanesulfonyl)imide salt (LiTFSI) in the melt state through small-angle neutron scattering (SANS) experiments. Scattering profiles from blends of hydrogenated and deuterated PEO mixed with LiTFSI were measured as a function of salt concentration. Scattering profiles from pure deuterated PEO/LiTFSI mixtures were used for background-subtraction purposes. The densities of PEO/LiTFSI mixtures of varying salt concentrations were measured to calculate partial molar monomer volumes of PEO and LiTFSI to account for nonideal mixing. Kratky plots of the scattering profiles were used to calculate the salt concentration dependence of statistical segment length. At low salt concentrations, segment length decreases with increasing salt concentration, before increasing with increasing salt concentration in the high salt concentration regime. The random phase approximation was used to predict theoretical scattering profiles from the calculated segment lengths and partial molar volumes; there is excellent agreement between the theoretical and measured scattering profiles at all salt concentrations. There appears to be a correlation between chain dimensions and coordination between lithium ions and EO monomers. The scattering profiles of the pure deuterated PEO/LiTFSI mixtures suggested the presence of ion clusters of characteristic size of 0.6 nm at high salt concentrations.



INTRODUCTION

Solid polymer electrolytes are of significant current interest due to their potential use in rechargeable lithium metal batteries.^{1–3} The most widely studied polymer electrolyte system is poly(ethylene oxide) (PEO) mixed with lithium bis(trifluoromethanesulfonyl)imide salt (LiTFSI), PEO/LiTFSI. It is well-known that the ether oxygens of the PEO backbone solvate Li ions, which leads to high ionic conductivity.^{4–6} The electrochemical and transport properties of PEO/LiTFSI have been fully characterized at temperatures above the melting temperature of PEO, e.g., 90 °C.^{7,8} Ion conduction in amorphous polymer electrolytes takes place through two mechanisms: ion hopping between the polymer chains and diffusion of the entire polymer chain, which is coordinated with the ions.⁹ It has been previously shown that, at high polymer molecular weights ($M_{\text{PEO}} \geq 4 \text{ kg mol}^{-1}$), ion conduction is attributed only to the ion-hopping mechanism and the conductivity reaches a plateau as a function of molecular weight.^{10,11} It is well-known that the ionic conductivity of PEO/LiTFSI increases with increasing salt concentration due to an increase in charge carriers, until it reaches a maximum at moderate salt concentrations.⁵ From

there, the conductivity decreases with increasing salt concentration, which has been attributed to the decrease in segmental dynamics of the PEO chains.^{9,12} As salt concentration increases, the monomeric friction coefficient of the PEO chain increases, which decreases the segmental motion of the polymer chains. The nonmonotonic relationship between salt concentration and ionic conductivity can be attributed to the exponential increase in the friction coefficient experienced by the PEO monomers.¹³

While there have been many theoretical and experimental studies conducted on the ion-transport mechanisms in PEO/LiTFSI, very few studies have focused on the effect of added salt on the size of the PEO chains. Annis and co-workers studied the effect of lithium iodide (LiI) salt on the radius of gyration, R_g , of PEO in the amorphous state.¹⁴ They showed through small-angle neutron scattering (SANS) experiments that, at a salt concentration of $r = 0.067$, where r is the molar ratio of Li to ethylene oxide (EO) repeat units ($r = \frac{[\text{Li}]}{[\text{EO}]}$),

Received: July 19, 2019

Revised: October 12, 2019

Published: November 7, 2019

there is a 10% decrease in R_g compared to the salt-free state at 90 °C. These results were qualitatively confirmed with accompanying molecular dynamics (MD) simulations. MD simulations have shown that the preferred conformation is the coordination of one Li ion to six EO and each Li ion is solvated by at most two PEO chains.^{15–17} This increases the population of gauche conformers, thereby reducing R_g .^{14,15,18} Accurate measurements of R_g , and therefore the statistical segment length, l ($l^2 = \frac{6R_g^2}{N}$), in salt-containing systems are important because they provide insight into the effect of salt on the polymer chain conformations. Unfortunately, the experimental data on this important subject is restricted to a single salt (LiI) and a single salt concentration ($r = 0.067$).

The purpose of this study is to systematically measure the effect of salt on the chain dimensions of PEO/LiTFSI in the melt state through SANS experiments. Our work covers salt concentrations in the range of $0 \leq r \leq 0.30$. In the low salt concentration regime, $r < 0.125$, l decreases monotonically with increasing salt concentration. However, in the high salt concentration regime, $r \geq 0.125$, l increases with increasing salt concentration. The SANS data suggest the presence of ion aggregates with characteristic dimensions of ~ 0.57 nm at high salt concentrations, $r \geq 0.25$.

MATERIALS AND METHODS

Electrolyte Preparation and Density Measurements. Electrolytes were prepared according to ref 7. The hydrogenous PEO (hPEO) and deuterated PEO (dPEO) (Polymer Source) used in this study have a molecular weight of 35 kg mol^{-1} and polydispersities of 1.08 and 1.09, respectively. All electrolytes are homogeneous mixtures of hPEO, dPEO, and LiTFSI (Sigma-Aldrich). Both isotopes of PEO as well as the LiTFSI were dried in a glovebox antechamber under vacuum at 90 and 130 °C for 1 and 3 days, respectively. Electrolytes were prepared by dissolving PEO and LiTFSI in anhydrous tetrahydrofuran (Sigma-Aldrich) and stirring at 60 °C until completely dissolved. The composition of the polymer blends was 10% dPEO/90% hPEO by volume (densities of dPEO and hPEO were assumed to be equivalent). The amount of salt was varied such that the r value ranged from values of 0.03 to 0.30. All polymer/salt solutions were transparent. The solvated electrolytes were subsequently stirred on a hot plate at 60 °C until dry and placed in a glovebox antechamber under vacuum for 24 h at 90 °C to remove any trace solvent. All dried electrolytes are transparent above 70 °C. Density measurements were conducted according to ref 7 and conducted at 90 °C on pure hPEO/LiTFSI mixtures for $0.18 \leq r \leq 0.28$ in 0.02 increments. Three measurements were taken, and the average measurement is reported. No measurements were taken for electrolytes with $r \geq 0.30$ because the system phase segregates.

SANS Sample Preparation and Experiments. SANS sample preparation was conducted in inert argon gloveboxes due to the hygroscopic nature of the Li salt. PEO/LiTFSI mixtures were melted into 1 in. inner diameter, 1 mm thick stainless-steel spacers placed on top of 1.5 mm thick, 25.4 mm outer diameter quartz windows (Esco Optics). Samples were degassed in the glovebox antechamber for 15 min at 90 °C before placing the second quartz window on top of the polymer. Quartz–polymer–quartz sandwiches were then sealed in custom-built, air-free titanium holders.

SANS experiments were conducted on the NG7 and NGB 30m beamlines at the National Institute of Standards and Technology Center for Neutron Research in Gaithersburg, MD. On both instruments, measurements were performed with a neutron wavelength of 6 Å, and three sample-to-detector distances of 13, 4, and 1 m were used. Neutron lenses were also used with neutron wavelengths of 8.4 Å on the NGB and 8.09 Å on the NG7, which allowed for access to a scattering wave-vector magnitude, $q = \left(\frac{4\pi}{\lambda}\right) \sin \frac{\theta}{2}$, ranging

from 0.03 to 4 nm^{-1} .¹⁹ A 0.5 in. aperture was used for all measurements. All measurements were conducted at 90 °C. On the NGB a 9-position Peltier cooling/heating block was used, and on the NG7 a 10-position heating block with a circulating fluid was used to maintain constant sample temperature. Samples of thickness of 1 mm were employed. The total scattering intensity was corrected for detector sensitivity, background, and empty cell contributions as well as sample transmission and thickness.^{20,21}

RESULTS AND DISCUSSION

The measured absolute SANS intensity, $I(q)$, for the 10% dPEO/90% hPEO/LiTFSI (referred to as blends) is shown in Figure 1a, as a function of the scattering vector, q (nm^{-1}). All

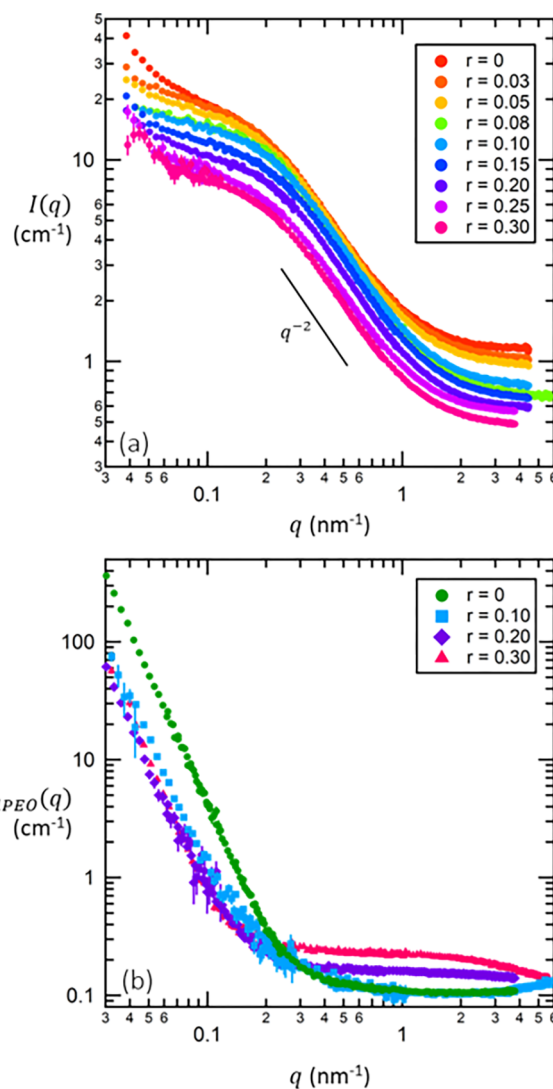


Figure 1. Measured absolute SANS intensity, $I(q)$, vs q (nm^{-1}) at 90 °C for (a) blends of hPEO/dPEO/LiTFSI and (b) pure dPEO/LiTFSI samples at varying salt concentrations, r . Error bars represent one standard deviation.

of the data in this study were taken at 90 °C, and error bars represent one standard deviation.^{20,21} The scattering profiles from all of the blends are similar. Adding salt mainly shifts the curves downward. At high q ($q > 2 \text{ nm}^{-1}$), the scattering profiles approach a plateau mainly due to incoherent scattering. In the range $0.2 < q$ (nm^{-1}) ≤ 0.9 , $I(q)$ is proportional to q^{-2} . The scattering intensity is a much weaker

function of q at $q < 0.2 \text{ nm}^{-1}$. All of these features are generally consistent with scattering from blends of hydrogenous and deuterated polymers obeying random walk statistics.

The measured absolute SANS intensities for the dPEO/LiTFSI mixtures, $I_{\text{dPEO}}(q)$, are shown in Figure 1b. We mainly use these data for background correction following ref 22. Note that the magnitude of the scattering intensity from the dPEO/LiTFSI samples at low q ($q < 0.1 \text{ nm}^{-1}$) is much larger than that of the blends. While high scattering from pure deuterated samples has been seen previously,²³ the reason for this observation has not been fully established. We believe that the scattering intensity of the pure deuterated sample is higher than that of the salt-containing samples due to its higher concentration of dPEO, the main contributor to high-intensity scattering. At high q in Figure 1b, we see a plateau that is independent of salt concentration when $r < 0.10$. The plateau rises at higher salt concentrations.

Following the analysis in ref 22, the data in Figure 1b were used to subtract the scattering from the fully deuterated chains from the scattering intensity of the blends (Figure 1a) to obtain the coherent scattering intensity,

$$I_{\text{coh}}(q, r) = I(q, r) - fI_{\text{dPEO}}(q, r) - I_{\text{inc}}(q, r) \quad (1)$$

where f is the volume fraction of dPEO ($f = 0.1$) and $I_{\text{inc}}(q)$ is the estimated incoherent scattering from hydrogen atoms in our samples calculated using software provided by NIST.²⁰ Note that the coherent scattering intensity at a given value of r is obtained after subtracting $I_{\text{dPEO}}(q, r)$ at the same r -value. When $I_{\text{dPEO}}(q, r)$ was not measured for specific values of r , the interpolated scattering profiles obtained using the weighted average between the appropriate salt concentrations was used. The interpolated scattering profiles for all of the salt concentrations are provided in the Supporting Information (Figure S11).

Figure 2 shows the coherent SANS intensities, $I_{\text{coh}}(q)$, for all salt concentrations. The relationship between scattering intensity and salt concentration seen in the raw data (Figure 1a) persists for $I_{\text{coh}}(q)$: mixtures with lower salt concentrations

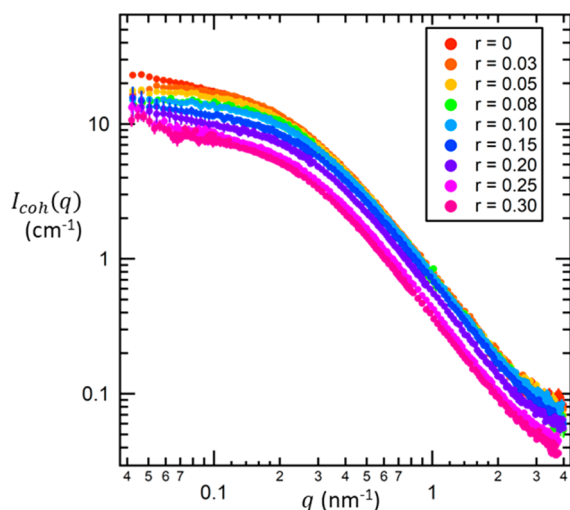


Figure 2. Coherent SANS intensity, $I_{\text{coh}}(q)$, for the blends after dPEO background subtraction taken at $90 \text{ }^\circ\text{C}$ for varying salt concentrations, r , as a function of the scattering vector, q (nm^{-1}). Error bars represent the standard deviation of the scattering data.

have a higher scattering intensity. Error bars represent the standard deviation of the scattering data.

The coherent scattering intensity for a homogeneous polymer blend can be calculated using the random phase approximation (RPA).^{24–28} We assume that the isotopic interaction parameter, $\chi_{\text{dPEO/hPEO}}$, as well as the interaction parameter between PEO and LiTFSI, $\chi_{\text{PEO/LiTFSI}}$, is negligible and that the salt is randomly distributed throughout the solution. Under these approximations, the coherent scattering intensity is given by

$$I_{\text{coh}}(q) = (B_1 - B_2)^2 \left(\frac{S_{11}S_{22}}{S_{11} + S_{22}} \right) \quad (2)$$

where component 1 is hPEO, component 2 is dPEO, B_i is the neutron scattering length density of component i given by $B_i = \frac{b_i}{\bar{v}_i}$, and \bar{v}_i and b_i are the partial molar monomer volumes and neutron scattering lengths of component i , respectively. The neutron scattering lengths of hPEO and dPEO are 4.13×10^{-13} and 4.58×10^{-12} cm, respectively. Partial molar monomer volumes, \bar{v}_i , were used to account for the nonideal mixing between PEO and LiTFSI if it exists.⁷ We note in passing that mixtures of salts and low molecular weight liquids exhibit large volume change of mixing.²⁹ The structure factor, S_{ij} is given by

$$S_{ii} = \phi_i N_i \bar{v}_i P(q) \quad (i = 1, 2) \quad (3)$$

where ϕ_i is the volume fraction of component i , N_i is the degree of polymerization of component i , and

$$P(q) = 2 \left[\frac{\exp(-x) - 1 + x}{x^2} \right] \quad (4)$$

with $x = q^2 R_g^2$. We assume that the monomer volume and degree of polymerization are the same between the hydrogenated and deuterated PEO samples (e.g., $N_{\text{hPEO}} = N_{\text{dPEO}} = N = 795$). Both components are modeled as flexible Gaussian chains and

$$R_g^2 = \frac{Nl^2}{6} \quad (5)$$

where l is the statistical segment length of both hPEO and dPEO. Note that the reference volume was taken to be the monomer volume for PEO, \bar{v}_{EO} . The polymer volume fractions are given by

$$\phi_1 = (1 - f)\phi_p \quad (6)$$

and

$$\phi_2 = f\phi_p \quad (7)$$

where ϕ_p is the volume fraction of polymer in the PEO/LiTFSI mixture calculated from $\phi_p = 1 - \phi_{\text{LiTFSI}}$ and

$$\phi_{\text{LiTFSI}} = x_{\text{LiTFSI}} \frac{\bar{v}_{\text{LiTFSI}}}{\nu_{\text{EO,salt}}} \quad (8)$$

where $\nu_{\text{EO,salt}}$ is defined as the volume occupied by a mole of a given PEO/LiTFSI mixture divided by Avogadro's number, x_{LiTFSI} is the mole fraction of salt given by

$$x_{\text{LiTFSI}} = \frac{r}{1 + r} \quad (9)$$

and $\nu_{\text{EO,salt}}$ was calculated according to

$$\nu_{\text{EO,salt}} = \frac{(1 - x_{\text{LiTFSI}})M_{\text{EO}} + x_{\text{LiTFSI}}M_{\text{LiTFSI}}}{\rho(x_{\text{LiTFSI}})N_{\text{av}}} \quad (10)$$

where M_{EO} and M_{LiTFSI} are the molar masses of EO and LiTFSI, 44.05 and 287.09 g mol⁻¹, respectively, and N_{av} is Avogadro's number.

Figure 3a shows $\rho(x_{\text{LiTFSI}})$, the density of a given PEO/LiTFSI mixture, measured at 90 °C as a function of salt mole

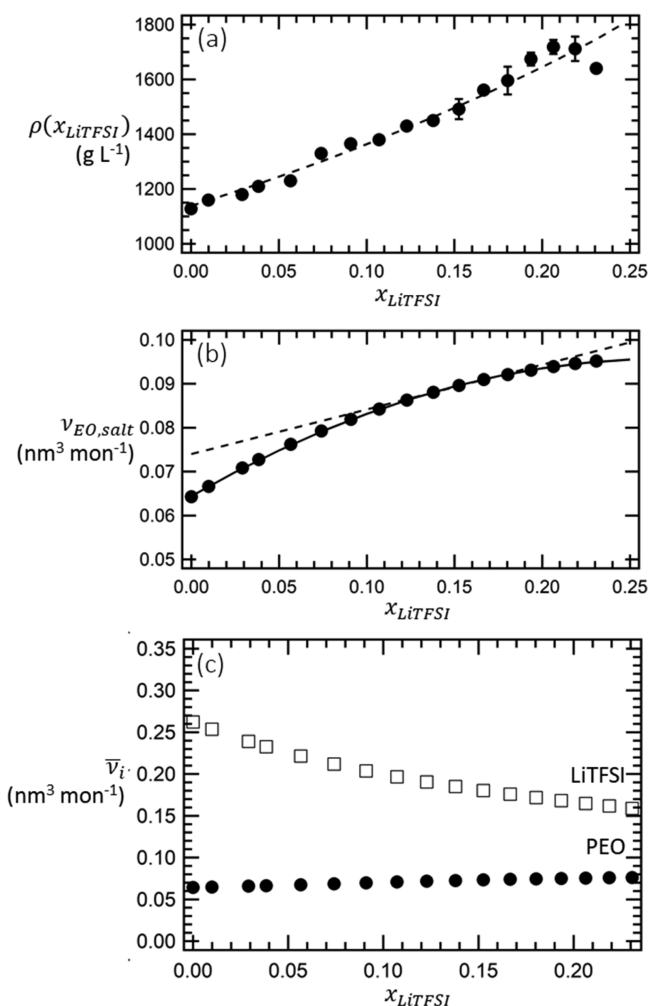


Figure 3. Properties of PEO/LiTFSI mixtures at 90 °C. (a) Dependence of density, $\rho(x_{\text{LiTFSI}})$, on salt mole fraction, x_{LiTFSI} . Error bars represent the standard deviation of measured samples. Molar properties are calculated on the basis of EO monomers (not PEO chains). (b) Volume occupied by a mole of a given PEO/LiTFSI mixture divided by Avogadro's number, $\nu_{\text{EO,salt}}$, as a function of salt mole fraction, x_{LiTFSI} . Solid curve represents eq 10, and the dashed line is an example of a tangent, constructed at $r = 0.20$ using eq 12. (c) Partial molar volumes of EO monomer (circles), as well as LiTFSI (squares) divided by Avogadro's number as a function of salt mole fraction, x_{LiTFSI} . These volumes are used to compute the scattering length densities and volume fractions of the two components in our mixture.

fraction, x_{LiTFSI} . Some of the data in Figure 3a were taken from ref 7. It is evident that $\rho(x_{\text{LiTFSI}})$ is approximately a linear function of x_{LiTFSI} ; the dashed line in Figure 3a is a linear fit through the data:

$$\rho(x_{\text{LiTFSI}}) = Ax_{\text{LiTFSI}} + B \quad (11)$$

The fit in Figure 3a gives $A = 2635 \text{ g L}^{-1}$ and $B = 1114 \text{ g L}^{-1}$. Equations 10 and 11 were used to calculate $\nu_{\text{EO,salt}}$ and this parameter is plotted as a function of x_{LiTFSI} in Figure 3b. The solid curve in Figure 3b represents a continuous function obtained by combining eqs 10 and 11. The values of partial molar volumes, $\bar{\nu}_{\text{EO}}$ and $\bar{\nu}_{\text{LiTFSI}}$, at a given salt concentration are calculated by constructing tangents to the solid curve in Figure 3b at that salt concentration and noting the intercepts at $x_{\text{LiTFSI}} = 0$ and 1, respectively.³⁰ The slope of tangent is given by the analytical expression

$$\frac{d\nu_{\text{EO,salt}}}{dx_{\text{LiTFSI}}} = \frac{B[M_{\text{LiTFSI}} - M_{\text{EO}}] - AM_{\text{EO}}}{N_{\text{av}}(Ax_{\text{LiTFSI}} + B)^2} \quad (12)$$

An example of a tangent is shown for $r = 0.20$ as a dashed line in Figure 3b. The partial molar volumes thus obtained are plotted as a function of x_{LiTFSI} in Figure 3c. The partial molar volumes of both components are monotonic functions of salt concentration. We found that $\bar{\nu}_{\text{EO}}$ increases with increasing salt concentration from $\bar{\nu}_{\text{EO}} = 0.064$ to $0.076 \text{ nm}^3 \text{ mon}^{-1}$ from $r = 0$ to 0.30. In contrast, $\bar{\nu}_{\text{LiTFSI}}$ exhibits a more pronounced dependence on salt concentration, decreasing with increasing salt concentration from 0.26 to $0.16 \text{ nm}^3 \text{ mon}^{-1}$ in the same salt-concentration window. In a previous study, where volume change of mixing was ignored, the values of volumes used were $\nu_{\text{EO}} = 0.069 \text{ nm}^3 \text{ mon}^{-1}$ and $\nu_{\text{LiTFSI}} = 0.24 \text{ nm}^3 \text{ mon}^{-1}$.³¹ To our knowledge, the data presented in Figure 3 represents the most exhaustive measurement of density as a function of salt concentration in PEO/LiTFSI mixtures.

On the basis of eqs 2–10, eq 2 can be rewritten as

$$I_{\text{coh}}(q) = (B_1 - B_2)^2 \phi_p f(1 - f) \bar{\nu}_{\text{EO}} NP(q) \quad (13)$$

Note that all of the parameters on the right side of eq 13 have been determined independently except for l , which is found in $P(q)$. We do not expect LiTFSI to have any preference for dPEO relative to hPEO. Thus, the scattering length density of LiTFSI is irrelevant. In addition, $I_{\text{coh}}(q)$ is directly proportional to ϕ_p , which monotonically decreases with salt concentration. Equation 13 explains the trend in low- q SANS intensity seen in Figures 1 and 2, where $I(q = 0)$ decreases with increasing salt concentration due to the decrease in polymer concentration, which is the main contributor to scattering in these systems.³² It is convenient to define the structure factor, $S(q)$, as

$$S(q) = \frac{I_{\text{coh}}(q)}{(B_1 - B_2)^2} \quad (14)$$

In the limit of large q , $S(q)$ is proportional to q^{-2} , and thus the product $q^2 S(q)$ is given by^{33,34}

$$\frac{q^2 S(q)}{\bar{\nu}_{\text{EO}}} = \frac{12 \phi_p f(1 - f)}{l^2} \quad (15)$$

Figure 4a shows a plot of $\frac{q^2 S(q)}{\bar{\nu}_{\text{EO}}}$ versus q for different salt concentrations. Such plots are referred to as Kratky plots.³⁵ The Kratky plots in Figure 4a are typical of polymeric samples. They begin at the origin and level off to give a plateau at intermediate q , and at large q values ($q > 2 \text{ nm}^{-1}$), we see deviations from the plateau. All of the features except the high- q deviations are consistent with eq 13. On monomeric length scales, deviations from random-walk statistics become evident

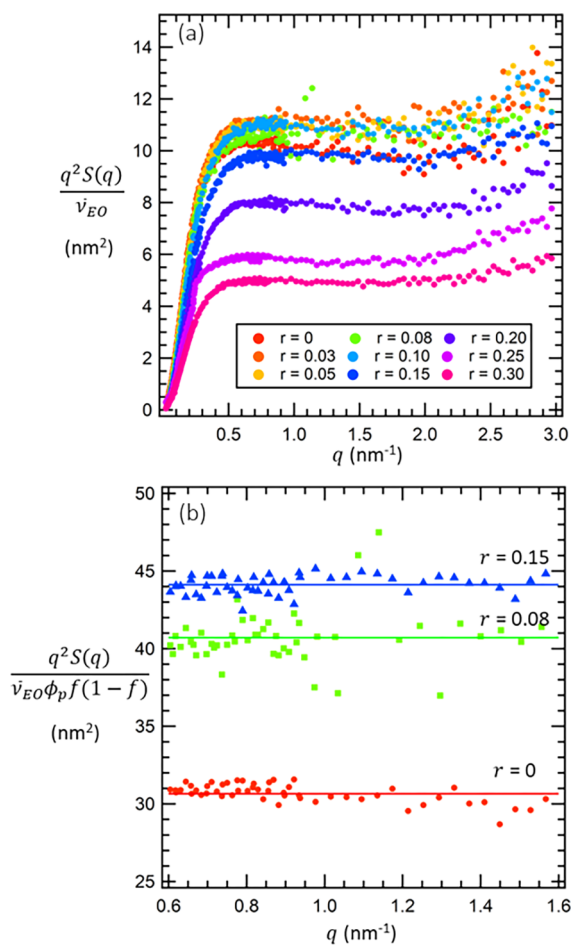


Figure 4. (a) Kratky plots, $\frac{q^2 S(q)}{v_{EO}}$, and (b) normalized Kratky plots, $\frac{q^2 S(q)}{v_{EO} \phi_p f (1-f)}$, vs q (nm^{-1}), for the blends at different salt concentrations. Error bars represent the standard deviation of the scattering data and are smaller than the symbols.

due to correlations between neighboring bonds within a repeat unit.³⁶

The height of the intermediate- q plateau of a Kratky plot can be used to determine l as all other parameters in eq 14 have been independently determined.³⁷ It is important to note that the height of the plateau does not decrease monotonically with salt concentration like the scattering profiles seen in Figures 1 and 2. For example, the Kratky plateau for $r = 0$ is not that different from that of $r = 0.15$ (Figure 4a). To focus on this fact, Figure 4b shows normalized Kratky plots where $\frac{q^2 S(q)}{v_{EO} \phi_p f (1-f)}$ is plotted versus q for selected salt concentrations in the q range where the Kratky plateau is observed ($0.6 \leq q$ (nm^{-1}) ≤ 1.6). Normalized Kratky plots for the remaining salt concentrations are provided in the Supporting Information (Figure SI2). The symbols in Figure 4b represent the SANS data, and the solid horizontal lines show the averaged value of $\frac{q^2 S(q)}{v_{EO} \phi_p f (1-f)}$ in the range of $0.6 < q$ (nm^{-1}) < 1.6 . This value is then used to determine l using eq 15.

In a related study, Hayashi et al.³⁸ studied mixtures of deuterated and hydrogenated polyisobutylene as a function of composition. They used an expression similar to eq 15 to

analyze their data and found that the plateau in the normalized Kratky plot was independent of composition, indicating that the statistical segment length of that system was also independent of composition. This is clearly not the case in the present study (Figure 4b).

Figure 5 shows the results for the salt-concentration dependence of the statistical segment length, l (left axis),

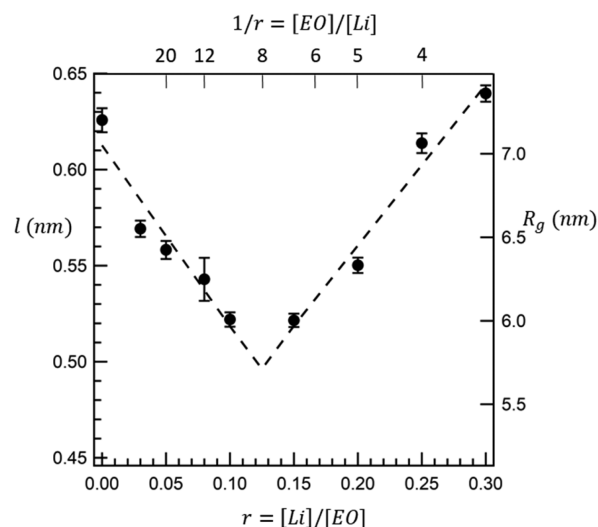


Figure 5. Statistical segment length, l (nm) (left axis), and radius of gyration, R_g (nm) (right axis), of PEO/LiTFSI blends at 90 °C as a function of salt concentration. l was calculated according to eq 15 from the Kratky plateau values, and R_g was calculated according to eq 5. Error bars represent the standard deviation between the data and the fit in Figure 4b. The top y-axis shows selected values of $1/r$, which quantifies the ratio of Li ions to EOs.

calculated using eq 15 and the normalized Kratky plateau (Figure 4b). The right axis of Figure 5 shows the salt-concentration dependence of the radius of gyration, R_g (right axis), calculated with eq 5. Error bars represent the standard deviation between the data and the fit in Figure 4b. The PEO statistical segment length decreases linearly upon salt addition in the range $0 < r < 0.125$, before linearly increasing with increasing salt concentration. The dashed lines in Figure 5 represent two linear regressions through the data at $r \leq 0.125$ and $r \geq 0.125$. The magnitude of the slope of these lines is approximately equal, and it appears that the maximum reduction in l might occur at $r = 0.125$ where the two dashed lines intersect. The statistical segment length at this salt concentration is 19% lower than that of neat PEO. At $r = 0.067$, there is a 10% decrease in segment length relative to the neat state, which is in excellent agreement with refs 14 and 15 where the decrease in segment length relative to the neat state in PEO/LiI mixtures at $r = 0.067$ is also 10%.

The top y-axis in Figure 5 plots selected values of $1/r$, which quantifies the number of EO present per Li atom. MD simulations of dilute mixtures of Li salts in PEO show that the Li ions are each coordinated with six ether oxygens.⁵ In other words, when $1/r = 6$, all of the oxygen atoms in the mixture are coordinated with Li ions. It is difficult to pinpoint the exact location of the crossover from chain contraction to chain expansion using the data in Figure 5; however, we believe it is close to $r = 0.125$ as denoted by the dashed lines in Figure 5, which intersect at $1/r = 8$. There appears to be a correlation

between chain dimensions and coordination between lithium ions and EO monomers.

Figure 6 shows the comparison between theory and experimental data for the PEO/LiTFSI mixtures at selected salt concentrations: (a) $r = 0$, (b) $r = 0.08$, and (c) $r = 0.15$ (the remaining salt concentrations are presented in the Supporting Information, Figure SI3). The circles represent

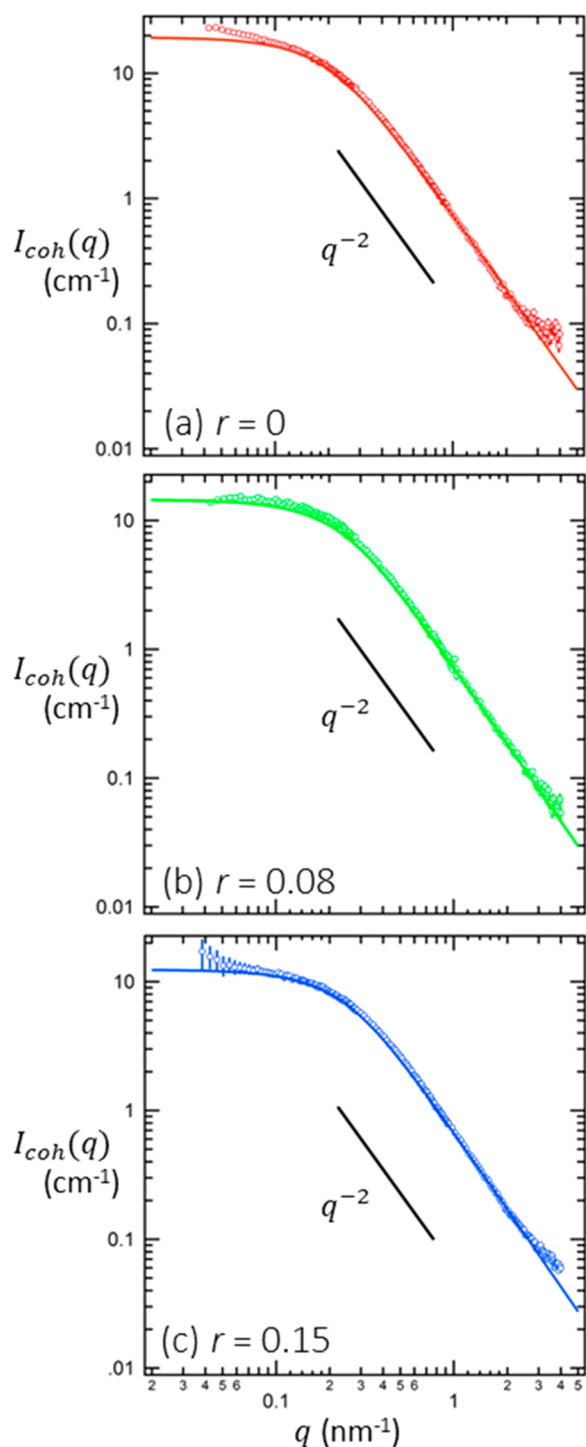


Figure 6. Comparisons between theoretical and experimental scattering profiles for (a) $r = 0$, (b) $r = 0.08$, and (c) $r = 0.15$. Circles represent the coherent SANS intensity reproduced from Figure 2, and the solid lines represent eq 13 when l was calculated according to eq 15. Error bars represent one standard deviation.

the coherent scattering data, $I_{\text{coh}}(q)$, reproduced from Figure 2, the solid curves represent eq 13 where l is obtained from the Kratky analysis (Figure 5) and all other parameters are determined independently. The agreement between theory and experiment is remarkable. The experimental data exhibit two regimes, a high- q Kratky regime where $I_{\text{coh}}(q)$ scales with q^{-2} and a low- q Zimm regime where $I_{\text{coh}}(q)$ is a weak function of q . The crossover between the Zimm and Kratky regimes is accurately predicted by eq 13. At $r = 0.08$, the measured $I_{\text{coh}}(q)$ at low q is very close to theoretical predictions. At $r = 0$ and $r = 0.15$, however, we see significant upturns in the scattering data that is inconsistent with eq 13. We attribute this to imperfect background subtraction. It is clear that the dPEO sample contains some impurity that gives rise to significant scattering at low q , which in turn complicates background subtraction.

Returning to Figure 1b, it is clear that the scattering profiles of dPEO/LiTFSI at $r \geq 0.20$ contain features at high q ($q > 0.2 \text{ nm}^{-1}$) that are absent in the samples with lower salt concentrations. We posit that these features arise due to the presence of ionic clusters. To investigate the nature of these clusters, the scattering from the neat dPEO was subtracted from the salt-containing samples:

$$I_{\text{clusters}}(q) = I_{\text{dPEO}}(q, r) - \phi_p I_{\text{dPEO}}(q, r = 0) \quad (16)$$

In Figure 7 we plot $I_{\text{clusters}}(q)$ versus q at different salt concentrations as circles. For $r \leq 0.20$, I_{clusters} is independent of

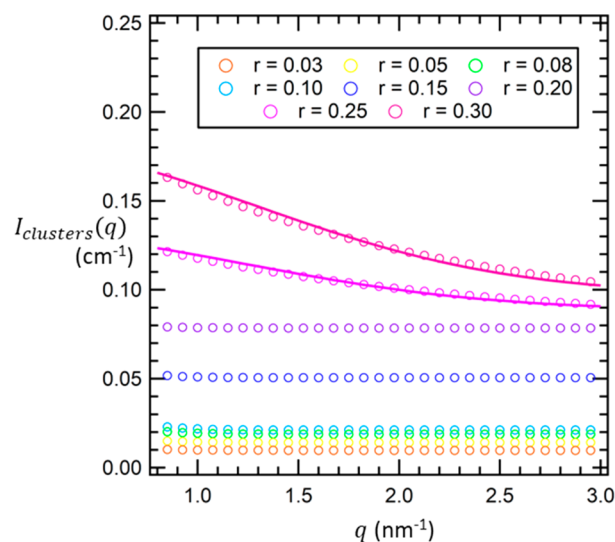


Figure 7. Scattering data from ion clusters, $I_{\text{clusters}}(q) = I(q, r) - \phi_p I(q, r = 0)$, for the pure dPEO/LiTFSI mixtures at high salt concentrations. Circles represent the data and lines represent a fit to eq 17. Only salt concentrations $r \geq 0.25$ could be fit to eq 17. Error bars represent the standard deviation of the scattering data and are smaller than the symbols.

q . The solid curves through the high salt concentration data ($r \geq 0.25$) are fits to

$$I_{\text{clusters}}(q) = \gamma_0 + I_0 \exp(-R^2 q^2) \quad (17)$$

which represents the Guinier equation for scattering from random irregular objects with characteristic size R .^{39,40} The origin of the background term, γ_0 , is not clear. The data in Figure 7 indicate that γ_0 increases monotonically with salt concentration, suggesting that the additional scattering in the dPEO/LiTFSI mixtures arises from the presence of salt. The

fact that $I_{\text{clusters}}(q)$ is q -independent for $r \leq 0.20$ may be an indication that the salt is uniformly distributed in the samples. The Guinier equation has been used to account for deviations from eq 13 at high- q for systems where structure overlaps with Debye scattering.⁴¹ The fitted parameters, y_0 and R , are similar for $r = 0.25$ and $r = 0.30$ (with $y_0 = 0.090 \pm 0.0004$ and 0.097 ± 0.0007 and $R = 0.58 \pm 0.01$ nm and 0.56 ± 0.01 nm for $r = 0.25$ and $r = 0.30$, respectively, where the error represents one standard deviation from the fits). However, I_0 is approximately twice as high for the $r = 0.30$ sample versus the $r = 0.25$ sample (0.04 ± 0.0006 vs 0.08 ± 0.0010 cm⁻¹, respectively, where the error represents one standard deviation from the fits). In theory, I_0 is proportional to the product of the volume fraction of aggregates and average aggregation number.^{41,42} The volume fraction of salt increases by 8% when r is increased from 0.25 to 0.30 (from 0.36 to 0.38). The measured value of I_0 suggests that the average aggregation number at $r = 0.30$ is a factor of 1.9 larger than that of $r = 0.25$; the average aggregate size remains constant at 0.57 nm between these two salt concentrations. These results are supported by MD simulations, which have shown that the number of ion clusters increases at these salt concentrations.^{15,16} Further characterization of ion clusters in PEO/LiTFSI using techniques such as X-ray scattering and Raman spectroscopy seem warranted.

CONCLUSIONS

We have determined the effect of added salt on the chain dimensions of PEO/LiTFSI mixtures through SANS experiments on ternary mixtures comprising hPEO, dPEO, and LiTFSI salt, conducted at 90 °C, above the melting transition of the mixtures. Scattering profiles were corrected for impurities present in the dPEO through background subtraction as described in ref 22. Partial molar volumes of EO and LiTFSI were calculated from measured density values in order to account for nonideal mixing between PEO and LiTFSI salt. The partial molar volume of EO increases with increasing salt concentration, while the partial molar volume of LiTFSI decreases with increasing salt concentration. The salt-concentration dependence of statistical segment length was calculated through the Kratky analysis of the intermediate- q scattering plateaus, which were normalized by polymer volume fraction. At low salt concentrations, $r < 0.125$, l linearly decreases with increasing salt concentration; in the high salt concentration region, $r \geq 0.125$, l increases with increasing salt concentration. When the calculated value of l is used in the random phase approximation, along with the independently determined partial molar monomer volumes and chain length, we see good agreement between theory and experiment. The SANS data suggested the presence of ion clusters of characteristic size of 0.57 nm in electrolytes with $r \geq 0.25$.

ASSOCIATED CONTENT

Supporting Information

The Supporting Information is available free of charge on the ACS Publications website at DOI: 10.1021/acs.macromol.9b01509.

Additional information on the details of dPEO background subtraction as well as scattering profiles for additional salt concentrations (PDF)

AUTHOR INFORMATION

Corresponding Author

*E-mail: nbalsara@berkeley.edu.

ORCID

Whitney S. Loo: 0000-0002-9773-3571

Nitash P. Balsara: 0000-0002-0106-5565

Notes

The identification of any commercial product or trade name does not imply endorsement or recommendation by the National Institute of Standards and Technology.

The authors declare no competing financial interest.

ACKNOWLEDGMENTS

This work was intellectually led by the Joint Center for Energy Storage Research (JCESR), an Energy Innovation Hub funded by the U.S. Department of Energy (DOE), Office of Science, Basic Energy sciences (BES), under Contract no. DEAC02-06CH11357. We acknowledge the support of the National Institute of Standards and Technology, U.S. Department of Commerce, in providing the neutron research facilities used in this work. Access to NGB-30m was provided by the Center for High Resolution Neutron Scattering, a partnership between the National Institute of Standards and Technology and the National Science Foundation under Agreement no. DMR-1508249. W.S.L. acknowledges funding from the National Science Foundation Graduate Student Research Fellowship DGE-1106400. We thank Paul Butler and Kevin Hou for helpful discussions.

LIST OF SYMBOLS

b_i	neutron scattering length of species i (cm mon ⁻¹)
B_i	scattering length density of species i (cm ⁻² mon ⁻¹)
C	electron density contrast (cm ⁻¹)
f	volume fraction of deuterated species
$I(q)$	scattering intensity (cm ⁻¹)
$I_{\text{coh}}(q)$	coherent scattering intensity (cm ⁻¹)
$I_{\text{inc}}(q)$	incoherent scattering intensity (cm ⁻¹)
$I_{\text{clusters}}(q)$	ionic cluster scattering intensity (cm ⁻¹)
l	statistical segment length (nm)
M_i	number-averaged molecular weight of species i (kg mol ⁻¹)
N_i	number-averaged degree of polymerization of species i (sites chain ⁻¹)
N_A	Avogadro's number
q	scattering vector (nm ⁻¹)
r	salt concentration ([Li] [EO] ⁻¹)
R_g	radius of gyration (nm)
$S(q)$	scattering structure factor
T	temperature (K)
x_i	mole fraction of species i

GREEK

ϕ_i	volume fraction of component i
χ	Flory–Huggins interaction parameter
ν_i	molar volume of species i divided by Avogadro's number (nm ³ mon ⁻¹)
$\bar{\nu}_i$	partial molar volume of species i divided by Avogadro's number (nm ³ mon ⁻¹)
ρ_i	density of species i (g cm ⁻³)

■ LIST OF ABBREVIATIONS

EO	ethylene oxide
LiTFSI	lithium bis(trifluoromethanesulfonyl) imide salt
MD	molecular dynamics
N_A	Avogadro's number
PEO	poly(ethylene oxide)
RPA	random phase approximation
SANS	small-angle neutron scattering

■ REFERENCES

- Armand, M. B. Polymer Electrolytes. *Annu. Rev. Mater. Sci.* **1986**, *16* (1), 245–261.
- Hallinan, D. T.; Balsara, N. P. Polymer Electrolytes. *Annu. Rev. Mater. Res.* **2013**, *43*, 503–525.
- Miller, T. F.; Wang, Z. G.; Coates, G. W.; Balsara, N. P. Designing Polymer Electrolytes for Safe and High Capacity Rechargeable Lithium Batteries. *Acc. Chem. Res.* **2017**, *50* (3), 590–593.
- Fenton, D. E.; Parker, J. M.; Wright, P. V. Complexes of Alkali Metal Ions with Poly(Ethylene Oxide). *Polymer* **1973**, *14* (11), 589.
- Lascaud, S.; Perrier, M.; Vallee, A.; Besner, S.; Prud'homme, J.; Armand, M. Phase Diagrams and Conductivity Behavior of Poly(Ethylene Oxide)-Molten Salt Rubbery Electrolytes. *Macromolecules* **1994**, *27* (25), 7469–7477.
- Mao, G.; Saboungi, M. L.; Price, D. L.; Armand, M. B.; Howells, W. S. Structure of Liquid PEO-LiTFSI Electrolyte. *Phys. Rev. Lett.* **2000**, *84* (24), 5536–5539.
- Pesko, D. M.; Timachova, K.; Bhattacharya, R.; Smith, M. C.; Villaluenga, I.; Newman, J.; Balsara, N. P. Negative Transference Numbers in Poly(Ethylene Oxide)-Based Electrolytes. *J. Electrochem. Soc.* **2017**, *164* (11), E3569–E3575.
- Villaluenga, I.; Pesko, D. M.; Timachova, K.; Feng, Z.; Newman, J.; Srinivasan, V.; Balsara, N. P. Negative Stefan-Maxwell Diffusion Coefficients and Complete Electrochemical Transport Characterization of Homopolymer and Block Copolymer Electrolytes. *J. Electrochem. Soc.* **2018**, *165* (11), A2766–A2773.
- Borodin, O.; Smith, G. D. Mechanism of Ion Transport in Amorphous Poly(Ethylene Oxide)/LiTFSI from Molecular Dynamics Simulations. *Macromolecules* **2006**, *39* (4), 1620–1629.
- Shi, J.; Vincent, C. A. The Effect of Molecular Weight on Cation Mobility in Polymer Electrolytes. *Solid State Ionics* **1993**, *60* (1–3), 11–17.
- Teran, A. a.; Tang, M. H.; Mullin, S. a.; Balsara, N. P. Effect of Molecular Weight on Conductivity of Polymer Electrolytes. *Solid State Ionics* **2011**, *203* (1), 18–21.
- Mao, G.; Saboungi, M. L.; Price, D. L.; Armand, M.; Mezei, F.; Pouget, S. α -Relaxation in PEO-LiTFSI Polymer Electrolytes. *Macromolecules* **2002**, *35* (2), 415–419.
- Mongcopa, K. I. S.; Tyagi, M.; Mailoa, J. P.; Samsonidze, G.; Kozinsky, B.; Mullin, S. A.; Gribble, D. A.; Watanabe, H.; Balsara, N. P. Relationship between Segmental Dynamics Measured by Quasi-Elastic Neutron Scattering and Conductivity in Polymer Electrolytes. *ACS Macro Lett.* **2018**, *7* (4), 504–508.
- Annis, B. K.; Kim, M. H.; Wignall, G. D.; Borodin, O.; Smith, G. D. Study of the Influence of LiI on the Chain Conformations of Poly(Ethylene Oxide) in the Melt by Small-Angle Neutron Scattering and Molecular Dynamics Simulations. *Macromolecules* **2000**, *33* (20), 7544–7548.
- Borodin, O.; Smith, G. D. Molecular Dynamics Simulations of Poly(Ethylene Oxide)/LiI Melts. 1. Structural and Conformational Properties. *Macromolecules* **1998**, *31* (23), 8396–8406.
- Fullerton-Shirey, S. K.; Maranas, J. K. Effect of LiClO₄ on the Structure and Mobility of PEO-Based Solid Polymer Electrolytes. *Macromolecules* **2009**, *42* (6), 2142–2156.
- Webb, M. A.; Jung, Y.; Pesko, D. M.; Savoie, B. M.; Yamamoto, U.; Coates, G. W.; Balsara, N. P.; Wang, Z. G.; Miller, T. F. Systematic Computational and Experimental Investigation of Lithium-Ion Transport Mechanisms in Polyester-Based Polymer Electrolytes. *ACS Cent. Sci.* **2015**, *1* (4), 198–205.
- Muller-Plathe, F.; van Gunsteren, W. F. Computer Simulation of a Polymer Electrolyte: Lithium Iodide in Amorphous Poly(Ethylene Oxide). *J. Chem. Phys.* **1995**, *103* (11), 4745–4756.
- Glinka, C. J.; Barker, J. G.; Hammouda, B.; Krueger, S.; Moyer, J. J.; Orts, W. J. The 30 m Small-Angle Neutron Scattering Instruments at the National Institute of Standards and Technology. *J. Appl. Crystallogr.* **1998**, *31* (3), 430–445.
- Kline, S. *SANS Data Reduction Tutorial*; NIST Center for Neutron Research: 2001.
- Kline, S. R. Reduction and Analysis of SANS and USANS Data Using IGOR Pro. *J. Appl. Crystallogr.* **2006**, *39* (6), 895–900.
- Balsara, N. P.; Lohse, D. J.; Graessley, W. W.; Krishnamoorti, R. Small-Angle Neutron Scattering by Partially Deuterated Polymers and Their Blends. *J. Chem. Phys.* **1994**, *100* (5), 3905–3910.
- Qiu, J.; Mongcopa, K. I.; Han, R.; López-Barrón, C. R.; Robertson, M. L.; Krishnamoorti, R. Thermodynamic Interactions in a Model Polydiene/Polyolefin Blend Based on 1,2-Polybutadiene. *Macromolecules* **2018**, *51* (8), 3107–3115.
- de Gennes, P. G. Theory of X-Ray Scattering by Liquid Macromolecules with Heavy Atom Labels. *J. Phys.* **1970**, *31* (2-3), 235–238.
- de Gennes, P. G. *Scaling Concepts in Polymer Chemistry*; Cornell University Press: Ithaca, NY, 1979.
- Akcasu, A. Z.; Tombakoglu, M. Dynamics of Copolymer and Homopolymer Mixtures in Bulk and in Solution via the Random Phase Approximation. *Macromolecules* **1990**, *23* (2), 607–612.
- Benoit, H.; Benmouna, M.; Wu, W.-L. Static Scattering from Multicomponent Polymer and Copolymer Systems. *Macromolecules* **1990**, *23*, 1511–1517.
- Hammouda, B. Random Phase Approximation for Compressible Polymer Blends. *J. Non-Cryst. Solids* **1994**, *172–174*, 927–931.
- Marcus, Y.; Hefter, G. Standard Partial Molar Volumes of Electrolytes and Ions in Nonaqueous Solvents. *Chem. Rev.* **2004**, *104* (7), 3405–3452.
- Smith, J. M.; Van Ness, H. C.; Abbot, M. *Introduction to Chemical Engineering Thermodynamics*, 7th ed.; McGraw-Hill Education: New York, 2004.
- Teran, A. a.; Balsara, N. P. Thermodynamics of Block Copolymers with and without Salt. *J. Phys. Chem. B* **2014**, *118* (1), 4–17.
- Kirste, R. G.; Kruse, W. A.; Ibel, K. Determination of the Conformation of Polymers in the Amorphous Solid State and in Concentrated Solution by Neutron Diffraction. *Polymer* **1975**, *16*, 120–124.
- Balsara, N. P.; Fetters, L. J.; Hadjichristidis, N.; Lohse, D. J.; Han, C. C.; Graessley, W. W.; Krishnamoorti, R. Thermodynamic Interactions in Model Polyolefin Blends Obtained by Small-Angle Neutron Scattering. *Macromolecules* **1992**, *25* (23), 6137–6147.
- Carsughi, F.; Bellmann, D.; Kulda, J.; Magnani, M.; Stefanon, M. Absolute Calibration of Small-Angle Neutron Scattering Data of a Double-Crystal Diffractometer. *J. Appl. Crystallogr.* **1997**, *30* (5), 857–861.
- Kratky, O. Possibilities of X-Ray Small Angle Analysis in the Investigation of Dissolved and Solid High Polymer Substances. *Pure Appl. Chem.* **1966**, *12* (1–4), 483–524.
- Daoud, M.; Cotton, J. P.; Farnoux, B.; Jannink, G.; Sarma, G.; Benoit, H.; Duplessix, C.; Picot, C.; de Gennes, P. G. Solutions of Flexible Polymers. Neutron Experiments and Interpretation. *Macromolecules* **1975**, *8* (6), 804–818.
- Crist, B.; Wignall, G. D. Small-Angle Neutron Scattering Studies of Chain Conformation in Semicrystalline Hydrogenated Polybutadiene. *J. Appl. Crystallogr.* **1988**, *21* (6), 701–706.
- Hayashi, H.; Flory, P. J.; Wignall, G. D. Configuration of the Polyisobutylene Chain According to Neutron and X-Ray Scattering. *Macromolecules* **1983**, *16* (8), 1328–1335.
- Guinier, A.; Fournet, G. *Small Angle Scattering of X-Rays*; John Wiley & Sons: New York, 1955.

- (40) Garetz, B. A.; Balsara, N. P.; Dai, H. J.; Wang, Z.; Newstein, M. C.; Majumdar, B. Orientation Correlations in Lamellar Block Copolymers. *Macromolecules* **1996**, *29* (13), 4675–4679.
- (41) Beaucage, G. Small-Angle Scattering from Polymeric Mass Fractals of Arbitrary Mass-Fractal Dimension. *J. Appl. Crystallogr.* **1996**, *29*, 134–146.
- (42) Bushell, G.; Amal, R. Measurement of Fractal Aggregates of Polydisperse Particles Using Small-Angle Light Scattering. *J. Colloid Interface Sci.* **2000**, *221* (2), 186–194.